On the validity of Avrami formalism in primary crystallization

Pere Bruna, Daniel Crespo, Ricard González-Cinca, and Eloi Pineda

Citation: Journal of Applied Physics **100**, 054907 (2006); doi: 10.1063/1.2337407
View online: http://dx.doi.org/10.1063/1.2337407
View Table of Contents: http://scitation.aip.org/content/aip/journal/jap/100/5?ver=pdfcov
Published by the AIP Publishing

On the validity of Avrami formalism in primary crystallization

Pere Bruna,[a] Daniel Crespo,[b] and Ricard González-Cinca[b]
Departament de Física Aplicada, EPSC, Universitat Politècnica de Catalunya, Avinguda del Canal Olímpic s/n, Castelldefels, Barcelona 08860 Spain

Eloi Pineda[b]
Departament de Física i Enginyeria Nuclear, ESAB, Universitat Politècnica de Catalunya, Avinguda del Canal Olímpic s/n, Castelldefels, Barcelona 08860 Spain

(Received 15 February 2006; accepted 24 June 2006; published online 11 September 2006)

Calorimetric data of primary crystallization is usually interpreted in the framework of the Kolmogorov [Dokl. Akad. Nauk SSSR **1**, 355 (1937)], Johnson and Mehl [Trans. AIME **135**, 416 (1939)], and Avrami [J. Chem. Phys. **7**, 1103 (1939); **8**, 212 (1940); **9**, 177 (1941)] (KJMA) theory. However, while the KJMA theory assumes random nucleation and exhaustion of space by direct impingement, primary crystallization is usually driven by diffusion-controlled growth with soft impingement between the growing crystallites. This results in a stop of the growth before the space is fully crystallized and induces nonrandom nucleation. In this work, phase-field simulations are used to check the validity of different kinetic models for describing primary crystallization kinetics. The results show that KJMA theory provides a good approximation to the soft-impingement and nonrandom nucleation effects. Moreover, these effects are not responsible of the slowing down of the kinetics found experimentally in the primary crystallization of glasses. © *2006 American Institute of Physics*. [DOI: 10.1063/1.2337407]

I. INTRODUCTION

The primary crystallization of undercooled liquids and glasses is one of the prevailing mechanisms of phase transformation into the solid state. In such transformations, precipitate particles with composition different from that of the amorphous matrix grow in a diffusion-controlled regime. The diffusion of one or more elements from or towards the crystalline phase is needed to achieve the adequate stoichiometry of the crystalline phase, and as a consequence concentration gradients of one or more elements appear in the boundaries of the crystalline particles. The theoretical analysis of diffusion-controlled grain growth have attracted considerable attention for many years. Such analyses have to deal with the troublesome problem of resolving the diffusion equation in the matrix, while satisfying boundary conditions in the moving precipitate-matrix interfaces. The diffusion equation,

$$D\nabla^2 c_m = \frac{\partial c_m}{\partial t}, \tag{1}$$

where D is the diffusion coefficient (assumed independent of the composition), rules the evolution of the concentration field $c_m = c_m(\mathbf{r},t)$ of a given component m in the amorphous matrix. The other main equation involved is the concentration flux balance at the moving interface,

$$(c_x - c_R)\frac{dR}{dt} = D\left(\frac{\partial c_m}{\partial r}\right)_{r=R}, \tag{2}$$

where R is the crystalline particle radius and $(\partial c_m/\partial r)_{r=R}$ is the concentration gradient in the amorphous phase side of the interface. Here, c_x is the concentration inside the crystalline precipitate, and c_R is the equilibrium concentration of the liquid phase at the interface of a particle of radius R. The dependence of c_R on the precipitate radius is determined by the capillarity condition,

$$c_R = c_l + c_l \Gamma \kappa, \tag{3}$$

where $\kappa = 2/R$ is the mean curvature in a growing sphere, c_l is the equilibrium concentration of the liquid phase, and Γ is the capillary length.

Even in the case of an isolated particle growing in an infinite matrix, exact analytical solutions of Eqs. (1) and (2) are only known if constant equilibrium concentration at the interface ($c_R = c_l$) is considered, that is, neglecting capillarity. The classical work of Zener[1] gives the exact solution for the case of spherical precipitates with boundary conditions,

$$\begin{aligned} &c_m(r=R,t)=c_l, \quad 0<t\leqslant\infty, \\ &c_m(r,t=0)=c_0, \quad 0<r\leqslant\infty, \\ &c_m(r=\infty,t)=c_0, \quad 0<t\leqslant\infty, \end{aligned} \tag{4}$$

where c_0 is the initial concentration of the matrix. However, even in such a case, the obtained solution is rather too cumbersome to use conveniently, and approximations giving simpler expressions are often used. In another classical reference, Aaron *et al.*[2] reviewed the different analytical approximations to the diffusion-controlled growth kinetics of

[a]Also at Centre de Recerca en Nanoenginyeria, UPC; electronic mail: pbruna@fa.upc.edu
[b]Also at Centre de Recerca en Aeronàutica, UPC.

single precipitate particles. The result is always a radius time dependence of the kind

$$R = \lambda(Dt)^{1/2}, \tag{5}$$

where λ is a dimensionless parameter depending on the value of the initial supersaturation,

$$\gamma = \frac{c_l - c_0}{c_l - c_x}. \tag{6}$$

The specific form of λ differs in each approximation.

These results do not take into account the destabilization of the interface. The spherical growth of precipitate particles is stable only for small particle sizes. In the case of $\gamma \ll 1$, the spherical shape is strictly stable in a size range going from R^* to $21R^*$, where R^* is the critical nucleation radius above which the sphere grows and below which it shrinks.[3] In such small radius range the capillarity effect is not negligible, thus invalidating the solutions presented above [Eq. (5)]. However, inside a range going from $10R^*$ to $100R^*$, spherical shape is not unduly unstable and diffusion-controlled growth of particles neglecting capillarity is a good approximation. Further growth above this range is governed by side-branching interaction leading to dendritic patterns.[4] Notwithstanding, particle growth as described by Eq. (5) is used in many works giving good results in the analysis of primary crystallization, as spherical particles showing diffusion-controlled growth are expected in the devitrification of many amorphous metallic alloys.[5,6]

When the precipitate particles reach a certain size, competition between neighboring particles begins to interfere with the growth. In polymorphic transformations this competition is purely geometric, that is, they stop growing because of direct impingement. In this case the overall transformation rate is well described by the Kolmogorov,[7] Johnson-Mehl[8] and Avrami (KJMA) equation,[7–9]

$$dx(t) = [1 - x(t)]d\tilde{x}(t), \tag{7}$$

or its integral counterpart,

$$x(t) = 1 - \exp[-\tilde{x}(t)]. \tag{8}$$

This equation relates the transformed volume fraction at a given time $x(t)$ with its extended counterpart $\tilde{x}(t)$. This extended transformed fraction is defined as the volume fraction occupied by the growing crystallites neglecting impingement, that is,

$$\tilde{x}(t) = \frac{4\pi}{3}\int_0^t I(\tau)R^3(\tau,t)d\tau, \tag{9}$$

where $I(\tau)$ is the crystallite nucleation rate per volume unit and $R(\tau,t)$ is the radius of a crystallite nucleated at time τ. In isothermal crystallization where the thermodynamic conditions determining the growth and nucleation laws are expected to be constant, it is possible to write the extended fraction as a power of time, that is,

$$x(t) = 1 - \exp(-kt^n), \tag{10}$$

where k is known as the reaction constant and n is the so-called Avrami exponent. The value of the Avrami exponent is then directly related to the time dependence of the growth and nucleation laws.[10]

When analyzing the results obtained from experimental data the Avrami exponent can be split in two parts, $n = n_I + n_G$, related, respectively, to the nucleation and growth mechanisms. In three-dimensional growth, n_I is expected to have values varying from 1 (constant nucleation rate) to 0 (preexisting or quenched-in nuclei) while n_G have typical values of 3 (constant growth rate) and 1.5 (parabolic or diffusion-controlled growth). Other more complex nucleation and growth mechanisms lead to values of the Avrami exponent different from the ones just mentioned. One should note here that different combinations of nucleation and growth mechanisms can lead to the same n value, with an adequate theoretical description to interpret the experimental crystallization data being necessary.[11]

The KJMA model is only valid for a random distribution of particle nuclei, isotropic growth with direct impingement, and particle growth rate not decreasing with time.[12,13] However, it is used as a good approximation in many transformations not strictly fulfilling these conditions due to its simplicity and robustness. Indeed, some approaches based on the KJMA equation [Eq. (8)] describe transformations with different kinds of nonrandom nucleation and anisotropic growth.[14–17]

Two main objections arise when applying the KJMA model to primary crystallization. Firstly, the parabolic growth law of Eq. (5) provides a growth rate decreasing with time, thus breaking one of the KJMA validity conditions. However, it has been demonstrated that the deviation of Eq. (8) in the prediction of the transformed fraction evolution for such a case is less than 0.9%,[14,16] so in this work we will consider that the KJMA model gives an adequate description of transformations with parabolic growth laws. Secondly, competition between neighboring particles through the overlap of concentration fields breaks some of the KJMA-model applicability requirements. On one hand, the growth of the particles does not stop because of direct impingement but gradually decreases due to the overlapping of the concentration profiles. The concentration gradients surrounding the particles become progressively flatter, thus reducing the diffusion-controlled growth rate. This is the so-called soft-impingement (SI) effect. In an analytical approach, Ham[18] found that the Avrami exponent keeps its value of $n = \frac{3}{2}$ (preexisting nuclei and diffusion-controlled growth) in the case of a regular array of spheroidal precipitate particles, but there is not one demonstration of the validity of the KJMA model for SI between not regularly distributed particles. On the other hand, the nucleation of crystallites is easier further away from previously existing ones, as the concentration gradients of the particles make the untransformed phase around the existing crystallites more stable to nucleation. This is the nonrandom nucleation (NRN) effect.[19,20] Neither SI nor NRN effects are taken into account in the KJMA model.

Indeed, the KJMA model, which is based on the geometrical interference between particles, can not be applied to transformations with low supersaturation values and so with final crystallized fractions $\gamma \lesssim 0.1$. In such cases, the behav-

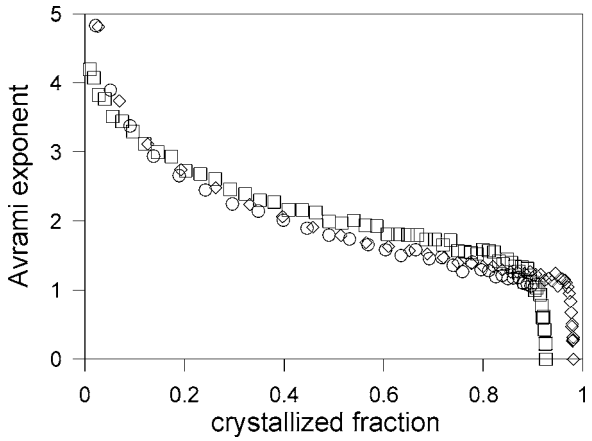

FIG. 1. Experimentally determined Avrami exponents vs crystallization fraction from Ref. 11 [annealing at 763 K (squares), at 773 K (hexagons), and at 783 K (circles)].

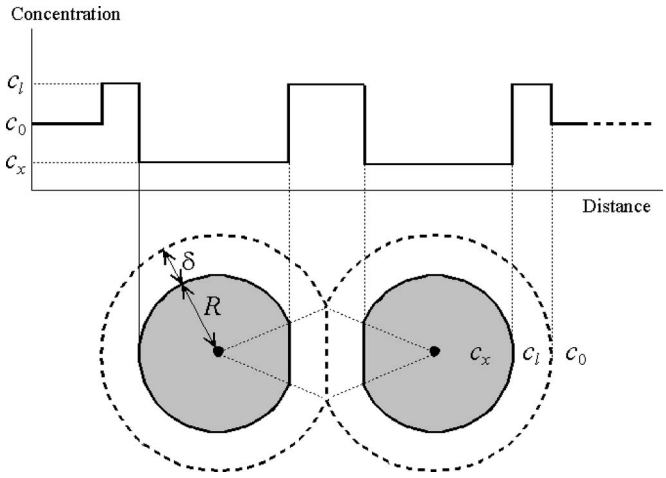

FIG. 2. Scheme of the geometrical model proposed to approximate the impingement between grains in primary crystallization.

ior of the kinetic parameters throughout the transformation can be well described by introducing a mean-field approach of the compositional change in the matrix.[21] However, in transformations with $\gamma \gtrsim 0.1$ some degree of geometric interference between growing grains is expected and, accordingly, primary crystallization was described classically by means of the KJMA equation.[22] In such cases the volume transformed fractions $x(t)$ and $\tilde{x}(t)$ are normalized by the final crystallized volume fraction, which corresponds to the initial supersaturation. Hence Eq. (8) is rewritten as

$$\xi(t) = 1 - \exp[-\tilde{\xi}(t)], \tag{11}$$

where $\xi = \gamma^{-1}x(t)$ and $\tilde{\xi} = \gamma^{-1}\tilde{x}(t)$.[10] The Avrami exponent is then calculated as

$$n(t) = \frac{d\ln\{-\ln[1-\xi(t)]\}}{d\ln(t)} = \frac{d\ln[\tilde{\xi}(t)]}{d\ln(t)}. \tag{12}$$

Equations (11) and (12) are widely used in studying the primary crystallization of amorphous alloys. Frequently, complex behavior and unusual low values of the Avrami exponent are reported.[23–25] Figure 1 shows an experimental determination of $n(\xi(t))$ from Ref. 11 where the Avrami exponent varies from $n \simeq 4$ at the initial stages of the transformation to $n < 1$ at the final stages. These low values are usually related to the SI and/or to the NRN,[6,14] with both effects expected to become specially important at the final stages of the transformation. However, as stated before, primary crystallization does not fulfill the validity conditions of the KJMA model.[12,13] Even more, the normalization by γ of both real and extended transformed volume fractions is not clearly justified.

The aim of this work is to test the validity of the KJMA model in a primary crystallization from the results obtained by means of phase-field model simulations. First, we will review two simple models which are first order approaches to the kinetics of a primary crystallization. Second, we will compare these kinetic models with the results of two- and three-dimensional phase-field model simulations of primary crystallization. In such simulations the NRN and SI effects are naturally included, then becoming a useful tool in checking the effects theoretically assigned to each phenomenon.

II. FIRST ORDER APPROACHES TO THE KINETICS OF PRIMARY CRYSTALLIZATION

In the following we will present two ways of approaching the SI and NRN effects described above, which we will refer to as geometrical and mean-field models.

A. The geometrical model

This model accounts for the geometrical distribution of the transformed phase and the surrounding stabilized matrix regions. It performs a simplified local mass balance of a growing crystalline grain, showing that the spherical regions resulting from this balance satisfy a KJMA-like relationship. A similar approach was already used by Shepilov in Ref. 26 with the assumption that the supersaturation should be small ($\gamma < 1$). In the present work we derive a relation between $x(t)$ and $\tilde{x}(t)$ valid for any value of γ.

Let us make a drastic simplification of the concentration profile around an isolated grain, substituting it by a completely stabilized boundary zone as sketched in Fig. 2. This stabilized boundary zone, with different thicknesses $\delta(\tau,t)$ for grains nucleated at different times τ, will be assumed to have an equilibrium concentration c_l. The thickness $\delta(\tau,t)$ can be obtained by means of a local mass balance from the volume of the corresponding transformed grain. This means that

$$R^3(\tau,t)(c_0 - c_x) = [[R(\tau,t) + \delta(\tau,t)]^3 - R(\tau,t)^3](c_l - c_0), \tag{13}$$

$$R_{\mathrm{TB}}(\tau,t) \equiv R(\tau,t) + \delta(\tau,t) = \gamma^{-1/3}R(\tau,t), \tag{14}$$

where R is the radius of the crystallite and R_{TB} is defined as the radius of the spherical *transformed plus boundary* zone including both the crystallized and the stabilized zones.

We will now define $x_{\mathrm{TB}}(t)$ as the volume fraction occupied by the transformed phase plus the stabilized boundaries around the growing grains. Neglecting impingement, each

individual crystalline grain plus its boundary region has a spherical shape, and consequently its behavior along the growth is the same as that of virtual *stable phase grains* of radius $R_{TB}(\tau,t)$. Thus, an *extended transformed plus boundary* volume fraction $\tilde{x}_{TB}$, can be defined as

$$\tilde{x}_{TB}(t) = (4\pi/3)\int_0^t I(\tau)[R_{TB}(\tau,t)]^3 d\tau = (4\pi/3)\int_0^t I(\tau)\gamma^{-1}R^3(\tau,t)d\tau \quad (15)$$

and, from Eqs. (9) and (15),

$$\tilde{x}(t) = \gamma\tilde{x}_{TB}(t). \quad (16)$$

Interference between the growing grains (SI effect) can now be treated including the stabilized boundary zone. The overlap of the concentration profiles responsible for the SI will be approximated by considering that the crystallite growth does not stop by direct interface impingement but because of the impingement of the stabilized boundary zones as sketched in Fig. 2. More precisely, let us define $\Omega_i(t)$, the free solid angle function of a certain crystalline grain i, as the solid angle of its boundary zone which has not impinged upon other neighbor boundary zones. Now, we will impose that the grain interface corresponding to this solid angle $\Omega_i(t)$ continues to grow unaffected by the impingement with the same growth law as an isolated grain, while the growth of the rest of the interface is utterly inhibited. Thus, we can express the transformed fraction due to the i grain as

$$x_i(t) = \int_\tau^t \Omega_i(t')R(\tau,t')^2 G(\tau,t')dt', \quad (17)$$

where $G(\tau,t)=dR(\tau,t)/dt$ is the growth rate at time t of a grain born at time τ. Therefore, the total transformed fraction will be

$$x(t) = \sum_{i=1}^{N(t)} x_i(t) = \sum_{i=1}^{N(t)} \int_\tau^t \Omega_i(t')R(\tau,t')^2 G(\tau,t')dt', \quad (18)$$

where $N(t)$ is the number of grains at time t.

Similarly, for the transformed plus boundary fraction, remembering that $R_{TB}(\tau,t)=\gamma^{-1/3}R(\tau,t)$, we obtain

$$x_{TB}(t) = \sum_{i=1}^{N(t)} x_{TB,i}(t) = \sum_{i=1}^{N(t)} \int_\tau^t \Omega_i(t')R_{TB}(\tau,t')^2 (dR_{TB}/dt')dt' = \gamma^{-1}\sum_{i=1}^{N(t)} \int_\tau^t \Omega_i(t')R(\tau,t')^2 G(\tau,t')dt'. \quad (19)$$

Then, from Eqs. (18) and (19), the actual transformed volume fraction is directly related to the transformed plus boundary volume fraction as

$$x(t) = \gamma x_{TB}(t). \quad (20)$$

The same expression is obtained, considering a global solute mass balance,

$$x(t)c_x + [x_{TB}(t) - x(t)]c_l + [1 - x_{TB}(t)]c_0 = c_0. \quad (21)$$

Although the untransformed matrix stabilization and the concentration profile overlap are dealt here with extreme simplification, the shape evolution of actual grains will be very similar to the one resulting from this approximation. Figure 2 shows that, in the proposed simplification, the facing grain interfaces are flat. Such flat interfaces are the result of direct impingement if the grains' radius follow a parabolic law $[R(\tau,t) \propto (t-\tau)^{1/2}]$ as expected in diffusion-controlled growth. In the actual physical situation these interfaces would not be flat, but the relationship between $x(t)$ and $x_{TB}(t)$ would hold equally because it is not dependent on the grain interface shapes, as shown by Eq. (21).

The NRN—the inhibition of nucleation in the boundary of existing grains—will be approximated in this model by assuming that nucleation is completely inhibited in the boundary area of completely stabilized untransformed matrix, while remaining unaffected in the rest of the untransformed volume. This is also a first order approximation because in a real system the nucleation probability would be related to the matrix concentration value, thus leading to a continuously decreasing nucleation probability when going from far away to near the crystalline grains.

As a consequence of the above assumptions, the evolution of x_{TB} can be seen as a process with random nucleation, isotropic growth rate $\gamma^{-1/3}G$, and direct impingement, which then satisfies a KJMA-like equation.[15] Thus, x_{TB} can be obtained from

$$\frac{dx_{TB}(t)}{d\tilde{x}_{TB}(t)} = 1 - x_{TB}(t), \qquad x_{TB}(t) = 1 - \exp[-\tilde{x}_{TB}(t)]. \quad (22)$$

Equations (16) and (20) allow us to rewrite the previous equation as

$$\gamma^{-1}x(t) = 1 - \exp[-\gamma^{-1}\tilde{x}(t)]. \quad (23)$$

This equation leads to a final value of transformed fraction equal to γ because of the exhaustion of the nonstabilized part of the untransformed volume as the crystallized plus stabilized volume occupy the whole space. Equation (23) is identical to Eq. (11), which is in fact the common way of using the KJMA theory in primary crystallization.[10] From the geometrical model just exposed, Eq. (11) is just a first order approximation for taking into account the SI and NRN effects.

B. The mean-field model

Another way for dealing with the stabilization of the untransformed matrix in primary crystallizations is the reduction of the kinetic parameters by means of a mean-field approach.[6] In order to account for the increase (or decrease) of the average concentration in the amorphous matrix as the transformation proceeds, a mean-field approach is adopted by introducing a time dependence on the average concentration in the untransformed matrix, $c_m(t)$. By means of a global mass balance,

$$x(t)c_x + [1 - x(t)]c_m(t) = c_0, \tag{24}$$

the mean supersaturation of the untransformed matrix variation can be written as

$$\frac{c_l - c_m(t)}{c_l - c_x} = \gamma \frac{1 - \gamma^{-1}x(t)}{1 - x(t)}, \tag{25}$$

where γ is the initial supersaturation given in Eq. (6). The factor $\varphi(t) = [1 - \gamma^{-1}x(t)]/[1 - x(t)]$, varying from $1 \to 0$ as $x(t)$ varies from $0 \to \gamma$, indicates the average stabilization of the matrix and is called the soft-impingement factor.

Considering that the driving force of the transformation is proportional to the supersaturation of the matrix, when the mean supersaturation decreases so does the driving force. Then, the kinetics of the primary crystallization can be modeled by introducing a decreasing driving force into the computation of the kinetic parameters, that is,

$$I(\gamma, t) \to I[\gamma\varphi(t), t] \tag{26}$$

and

$$G(\gamma, \tau, t) \to G[\gamma\varphi(t), \tau, t]. \tag{27}$$

It is worth saying here that different nucleation and growth models with empirically adjusted parameters are able to describe the kinetics of this kind of transformations. In fact, the approach described by the previous equations has been made by different authors, assuming diverse dependences of the kinetic parameters on the varying mean supersaturation of the matrix.[27] However, all that these models have in common is that the kinetic parameters become null at the end of the transformation, that is, $I \to 0$ and $G \to 0$ when $\gamma\varphi(t) \to 0$.

After taking into account the diminishing driving force in the kinetic parameter expressions, the geometrical impingement is modeled by means of the Avrami equation. Therefore, in this approach, the crystallized fraction given by the Avrami equation (8) reaches a final value of γ not because of the exhaustion of the untransformed volume but because of the vanishing of the kinetic parameters used for the calculation of the extended fraction, that is, $d\tilde{x}(t)/dt \to 0$ as $x(t) \to \gamma$.

Summarizing, this model accounts for the SI and NRN effects described above by considering the stabilization of the matrix a global process, while maintaining the applicability of the KJMA equation in order to deal with the geometric impingement. This is a first order approach and, although the mean reduction of the kinetic parameters has a physical sense, the applicability of the KJMA equation under these premises is of uncertain validity. On one hand, SI prevents direct impingement between the growing crystallites, against one of the main hypothesis of the KJMA theory. On the other hand, NRN is opposite to the random nucleation required by KJMA.

C. Actual kinetics of primary crystallization

The two first order approaches presented above are extremely opposite models accounting for the same phenomenon. The geometrical model deals with the stabilization of the untransformed matrix as a pure local effect, utterly modifying in some zones the nucleation and growth kinetics. On the contrary, the mean-field model deals with the stabilization of the matrix as a global effect equally affecting the nucleation and growth of all the growing crystallites. These two approaches are not able to account for the complex behaviors commonly observed in experimental transformed fraction curves of primary crystallization.[11,23–25]

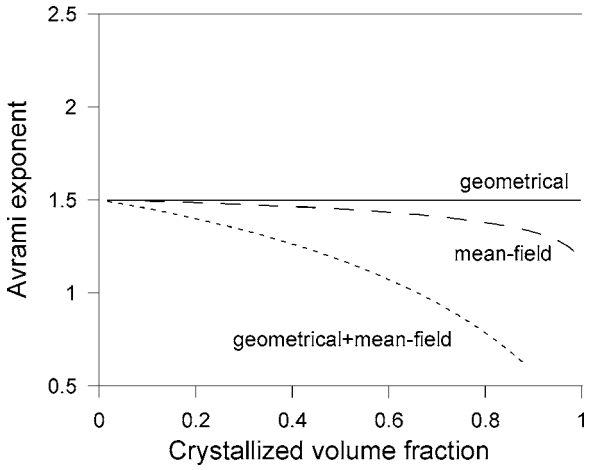

FIG. 3. Avrami exponents calculated using the geoemtrical and mean-field models in a transformation with diffusion-controlled growth.

As already stated, the analysis of primary crystallization is commonly performed using Eqs. (11) and (12), where the transformed fractions $x(t)$ and $\tilde{x}(t)$ are substituted by $\xi(t)$ and $\tilde{\xi}(t)$. A quick examination shows that it is not possible to give physical interpretations to these low Avrami exponents using *either* the geometrical model or the mean-field model described above. Figure 3 shows the Avrami exponents calculated using Eq. (12) for both the geometrical and the mean-field models in a transformation with preexisting nuclei and assuming a steady state diffusion-controlled growth given by

$$G(R) = \frac{D}{R}\frac{c_l - c_0}{c_l - c_x} = \gamma\frac{D}{R}, \tag{28}$$

which corresponds to Eq. (5) with $\lambda = [(c_l - c_0)/(c_l - c_x)]^{1/2}$. In the case of the mean-field model this growth rate is modified giving

$$G(R) = \frac{D}{R}\frac{c_l - c_m(t)}{c_l - c_x} = \frac{D}{R}\gamma\varphi(t). \tag{29}$$

One can observe that although the mean-field model predicts a decreasing exponent at the final stages of the transformation it is not able to account for the $n < 1$ values shown in Fig. 1. From the comparison of Figs. 1 and 3 it is clear that the first order approaches to the SI and NRN effects of the previous section are not able to describe the actual kinetics of primary crystallization in amorphous alloys.

Nevertheless, calorimetric data of primary crystallization of amorphous alloys were successfully described within the framework of the KJMA kinetics.[6] In this work the kinetics of primary crystallization in an amorphous metallic alloy were well described by a kinetic model, which is, in main terms, a juxtaposition of the geometrical and mean-field models discussed above. Experimental data on glass crystallization were interpreted by a mean-field reduction of the

kinetic parameters (very similar to the mean-field model above) plus a normalized KJMA equation (geometrical model). The dotted line in Fig. 3 shows that this combination of the geometrical and mean-field models (the *geometrical +mean-field* model) gives the low values of the Avrami exponent observed in experimental data. The model in Ref. 6 and other similar models available in literature[28,29] were defined as those accounting for the SI and NRN effects but, in fact, they are taking into account, although in first order approximations, two times such effects; they consider the stabilization of the untransformed matrix as a local geometrical phenomenon and also as global effect.

III. SIMULATIONS OF A PRIMARY CRYSTALLIZATION

Phase-field (PF) model simulations are a well-known tool in the study of solidification phenomena. In this work we have chosen a phase-field model already used in dendritic solidification[30,31] to simulate the transformation of a many-particle system without anisotropy in a diffusion-controlled regime. We use a phase-field model for solidification instead of recent phase-field models for nucleation[32,33] mainly for two reasons: (a) our aim is to study the interference between growing grains, not the nucleation of those grains that could be introduced externally with a known law, and (b) the used model does not introduce any extra complexity, allowing us to perform many-particle simulations consuming an acceptable computation time. In this model, a nonconserved order parameter or phase field ϕ (with values between 1 and 0 corresponding to untransformed and transformed regions, respectively) allows us to discriminate between the two phases. The interface dynamics is coupled to that of the dimensionless concentration field u (with values between -1 and 0 corresponding to the initial c_0 and equilibrium c_l concentrations of the matrix, respectively). The dimensionless equations of the model are

$$\frac{\epsilon^2}{m}\frac{\partial\phi}{\partial t} = \phi(1-\phi)\left[\phi - \frac{1}{2} + 30\epsilon\alpha\gamma u\phi(1-\phi)\right] + \epsilon^2\nabla^2\phi,$$
$$\frac{\partial u}{\partial t} + \frac{30}{\gamma}\phi^2(1-\phi)^2\frac{\partial\phi}{\partial t} = \nabla^2 u. \tag{30}$$

Paramaters ϵ, m, and α are related to the physical properties of the system as

$$\epsilon = \frac{W}{\omega}, \quad m = \frac{\mu\Gamma}{D}, \quad \alpha = \frac{\sqrt{2}\omega}{12\Gamma}, \tag{31}$$

where W is the dimensional interface width and μ is the kinetic coefficient. Equation (30) can be dimensionalized by choosing a typical length ω and a time scale given by

$$\tau = \frac{\omega^2}{D}. \tag{32}$$

The phase ϕ varies smoothly through the interface, and the sharp-interface model is recovered in the limit of vanishing ϵ. Simulations were performed using periodic boundary conditions in a 1000×1000 matrix for two dimensions and in a $450\times450\times450$ matrix for three dimensions, with $\gamma=0.2$ and $\gamma=0.5$ in each case. An explicit time-differencing scheme has been used to solve the equations for ϕ and u. Time and spatial discretizations were kept constant in all the simulations with values of $\Delta x=0.005$ and $\Delta t=2.5^{-6}$, and the phase-field parameters were fixed to $\epsilon=0.005$, $m=0.05$, and $\alpha=400$. The values of these parameters were chosen in order to minimize the transient stage in which the growth of grains is interface controlled. Moreover, to ensure the validity of these parameters we performed two tests: (a) the reduction of Δx does not change the results of the simulation and (b) the propagation rate of an interface in a phase transformation without diffusion reproduces the relation with the phase-field model parameters that in this case can be analytically calculated.[34,35]

In each simulation, up to 10^3 precipitate particles grow following the dynamics given by Eq. (30) which nucleate following an external, composition-dependent nucleation law. Details of the growth and nucleation laws will be given below in this section. The results presented in the next section correspond to the averaged output over ten simulations. This number of simulations ensures within a 95% of confidence an absolute error that follows a $M^{-1/2}$ law, where M is the number of simulations. According to the central limit theorem, performing more simulations will result in a reduction of the absolute error but without varying significantly the average. In all the simulations the transformed fraction is calculated as the ratio between the number of cells with $\phi<0.5$ and the total number of cells.

In the numerical simulation, the particles have a known growth law detailed in the next section and the evolution of the concentration field in the matrix follows Eq. (1). Hence, the effects of the stabilization of the untransformed matrix and the overlap of concentration fields of neighboring particles are naturally obtained. This will allow us to quantify the SI effect in a system with well-known nucleation and growth laws. It is worth noting here that the particle radius in the simulations are always in the size range in which the spherical shape is stable. Figure 4 shows a view of the transformed phase and concentration field evolution in a partial region of a two-dimensional simulation of preexisting nuclei growth, with supersaturation $\gamma=0.2$. The interference between precipitated particles due to the overlap of the concentration fields and the change in the matrix concentration are clearly observed. Analogously, Fig. 5 shows the transformed phase in a three-dimensional simulation of a system with the same nucleation protocol but with $\gamma=0.2$; in that view, an early stage of the transformation could be seen $[x(t)=0.003]$, so the soft-impingement effect is still not important.

A. Particle growth

Considering an isolated spherical particle, Eq. (30) yield a particle growth with two different stages. A transient interface-controlled growth, in which the concentration field is being progressively piled up at the particle/matrix interface, is followed by a diffusion-controlled regime with a growth law of the kind of Eq. (5). Figure 6 shows the radius and growth-rate evolution in a single particle simulation in

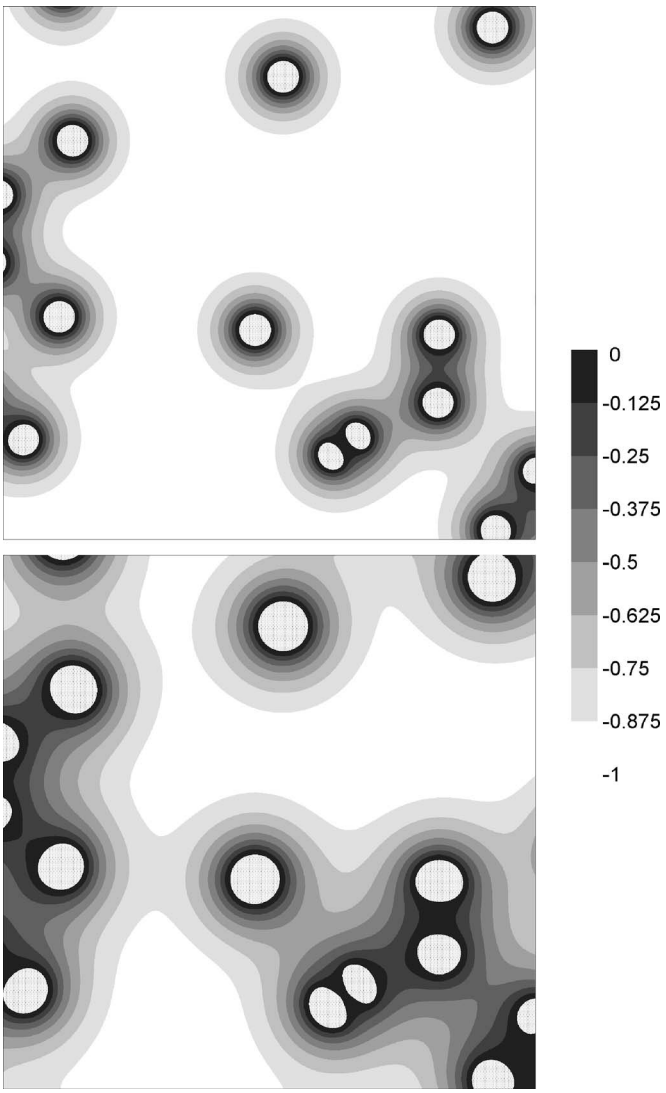

FIG. 4. Partial view of a two-dimensional (2D) simulation with preexisting nuclei at two different stages of the transformation ($x=0.06$ in the upper figure and $x=0.1$ in the lower). The gray gradient corresponds to the concentration (0 states for $c_m=c_l$ and -1 for $c_m=c_0$), whereas the dotted regions represent the crystallized phase.

three dimensions and with a supersaturation of 0.5. This particle growth is well described by the following time-dependent radius:

$$R(t) = R_i(t)\,\theta(t_c - t) + R_d(t)\,\theta(t - t_c), \tag{33}$$

where R_i and R_d are the radius time dependence for the interface-controlled and diffusion-controlled growths, respectively, and t_c is the time when the growth mechanism changes. R_i could be found by solving the following implicit equation:[34]

$$\frac{t}{v} = (R_i - R_0) + R^* \ln\left(1 + \frac{R_i - R_0}{R_0 - R^*}\right), \tag{34}$$

where R_0 is the initial radius and v is the asimptotic interface growth rate, which can be calculated analytically[34] and written in terms of γ and the phase-field model parameters: ϵ, α, and m.[35] R_d is found following Ref. 1 with the proper continuity conditions at t_c,

$$R_d = \sqrt{\lambda^2 Dt} - [\sqrt{\lambda^2 Dt_c} - R_i(t_c)].$$

As far as we know, any analytical result of the diffusion equation giving the value of λ in such conditions does not exist. So, in order to obtain the values of the parameter λ determining the diffusion-controlled growth rate for a given γ, we fitted the results of single particle PF-model simulations in two and three dimensions. The values obtained for $\lambda(\gamma)$ are close to the Zener solution[1] and can be seen in Table I. The differences arise from the transient growth stage not considered in Zener's classical work but present in the PF simulations and also expected in actual transformations. In addition to the value of λ, the shape of the concentration profiles obtained in the simulations is also close to Zener's analytical results. As the present work is focused on analyzing the interference among particles with diffusion-controlled growth, the parameters of the many-particle PF simulations were chosen with the aim of reducing, as much as possible, the influence of the transient growth stage on the overall kinetics.

B. Nucleation

We will consider two different nucleation protocols, namely, preexisting nuclei and continuous nucleation simulation. In the former case, a set of randomly distributed particle seeds starts growing with no further nucleation of particles. This case is widely found in the primary crystallization of glasses, where the annealing treatment activates the growth of already existing quenched-in nuclei. In the latter case, precipitate particles nucleate in the untransformed matrix all along the transformation, with a nucleation probability depending on the local concentration, thus yelding NRN.

In the continuous nucleation simulations, the nucleation rate of particles is controlled by a classical nucleation theory law[36] written as

$$I(c_m) = I_0 \exp\left\{-Q\left[\frac{1}{\ln^2(c_m/c_l)} - \frac{1}{\ln^2(c_0/c_l)}\right]\right\}. \tag{35}$$

The nucleation rate is utterly inhibited at the particle/matrix interface (where $c_m=c_l$) and has a value of I_0 at the matrix points with $c_m=c_0$. The value of I_0 is chosen to assure the nucleation of about 10^2-10^3 particles along the transformation. The parameter Q determines the extent of the nucleation inhibition around the particles.

The NRN effect on primary transformation kinetics was previously studied in detail by means of stochastic simulations. In Ref. 37, it was demonstrated that the effect on the overall kinetics is of second order compared to the effect of the growth-rate reduction due to SI. It was shown that the NRN modified significantly the transformation kinetics only in systems with nucleation inhibition over an extremely wide area surrounding the particles, and in such cases, the whole system could be considered very close to a preexisting nuclei transformation with no further nucleation after the initial stages.

In the present work, the value of Q is set in order that the number of nucleation events around an isolated precipitate

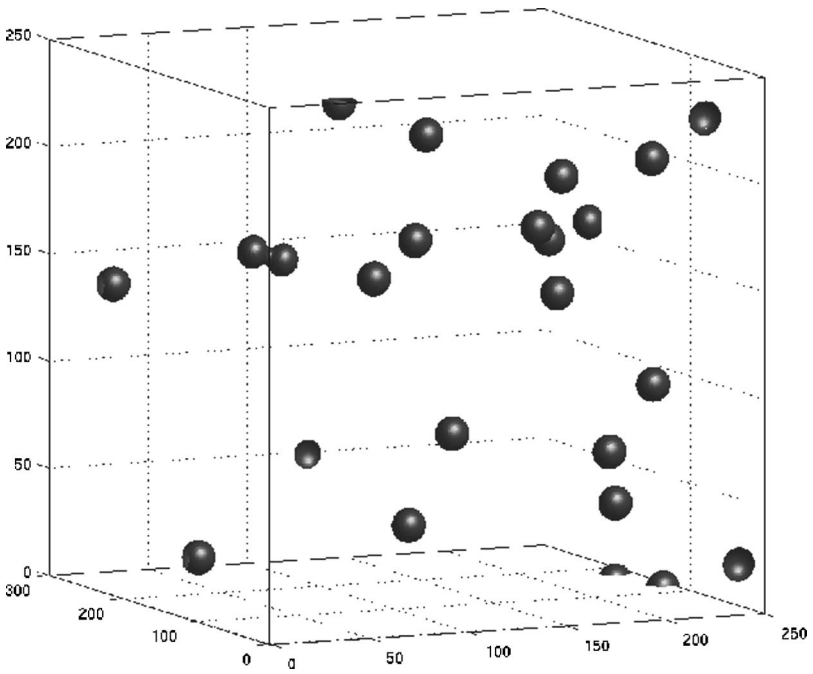

FIG. 5. Partial view of a 3D simulation with preexisting nuclei at an early stage of the transformation. The black spheres correspond to transformed phase.

particle with a Zener concentration profile,[1] which is similar to the concentration profiles generated in the PF simulations, coincides with the expected number for a steplike concentration profile, as it is considered in the geometrical model. Figure 7 shows the nucleation probability $I(c_m)/I_0$ for this Q value [$Q=0.0971$ for $\gamma=0.5$ in three dimensions (3D)] as a function of the distance from the precipitate particle nucleus. In this way, NRN is not expected to influence significantly the transformation kinetics, allowing the analysis of the SI effect in transformations with continuous nucleation. A detailed study of the effects on the transformation kinetics as function of Q is out of the purpose of this work. Some insight into this subject will be presented elsewhere.[35]

IV. RESULTS AND DISCUSSION

It is well known that nucleation and growth processes have scaling properties. Both the overall kinetics and the developed microstructure can be described in terms of dimensionless time and length parameters depending on the nucleation frequency and growth-rate values.[38,39] Therefore, the parameters defining the characteristics of the simulated transformations are just the final transformed volume fraction γ, the ratio between interface and diffusion growth rate, and (in the case of continuous nucleation) the nucleation parameter Q. The growth ratio rate determines the relative influence of the transient interface-controlled and the diffusion-controlled growth regimes over the particle total growth. As stated before, in this work v and D are chosen to reduce the interface-controlled regime influence as much as possible within the limitations of the simulation process. Parameter Q determines the relative size between the particles and the corresponding nucleation inhibited zone surrounding them; a lower Q value implies a smaller region where the nucleation is reduced [see Fig. 7 and Eq. (35)].

Figure 8 shows the transformed fraction evolution and the Avrami exponent behavior in the case of 125 preexisting nuclei and $\gamma=0.5$. The results of the simulations are compared with the geometrical and mean-field models described before. In these models, the nucleation and growth laws given by the simulation were used to calculate the extended transformed fraction $\tilde{x}(t)$. The geometrical+mean-field model, which is expected to qualitatively reproduce the features obtained in actual primary crystallization kinetics, is also depicted.

In both two- and three-dimensional simulations the

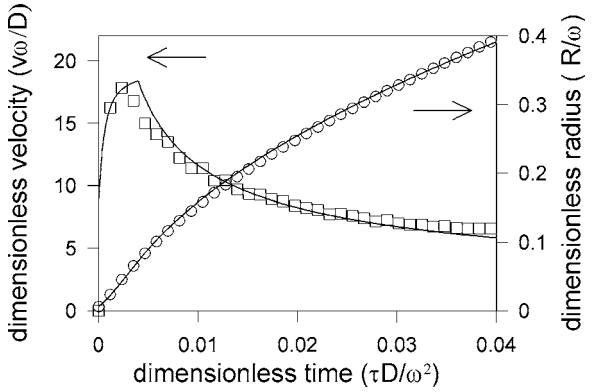

FIG. 6. Time evolution of the radius (circles) and its velocity (squares) obtained from a three-dimensional phase-field model simulation. Solid lines correspond to the analytical result from Eq. (37).

TABLE I. Values for the constant λ according to Ref. 1 and obtained from the simulations (λ_{sim}) for $\gamma=0.2$ and $\gamma=0.5$ and the dimensionality. The relation between λ and λ_{sim} is independent of the dimensionality, thus depending only on the supersaturation value.

	2D		3D		
γ	λ_{sim}	λ	λ_{sim}	λ	λ_{sim}/λ
0.2	0.660	0.629	0.953	0.908	1.05
0.5	1.757	1.562	2.335	2.076	1.125

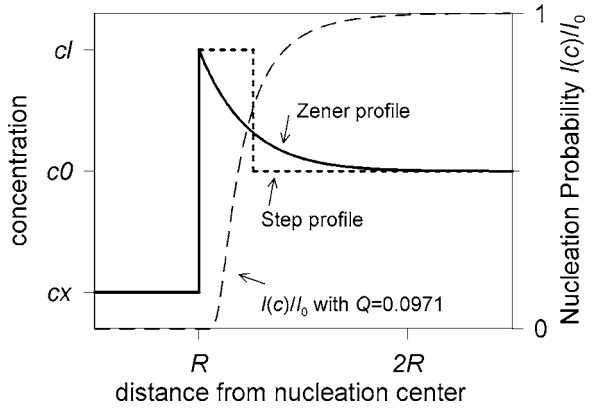

FIG. 7. Nucleation probability in 3D for $\gamma=0.5$ and $Q=0.0971$ as a function of the distance from the nucleation center (dashed line). Concentration profile according to Ref. 1 (solid line) and concentration profile according to the geometrical model (bold dashed line).

simple models described before reproduce with accuracy the $x(t)$ evolution. The geometrical model and, specially, the mean-field model give a very good agreement with the simulation results, while the geometrical+mean-field model gives slower kinetics. With that particular value of supersaturation the mean-field model is always slower than the geometrical model, and it fits perfectly the transformed fraction obtained by means of the simulation. This is not a general result;

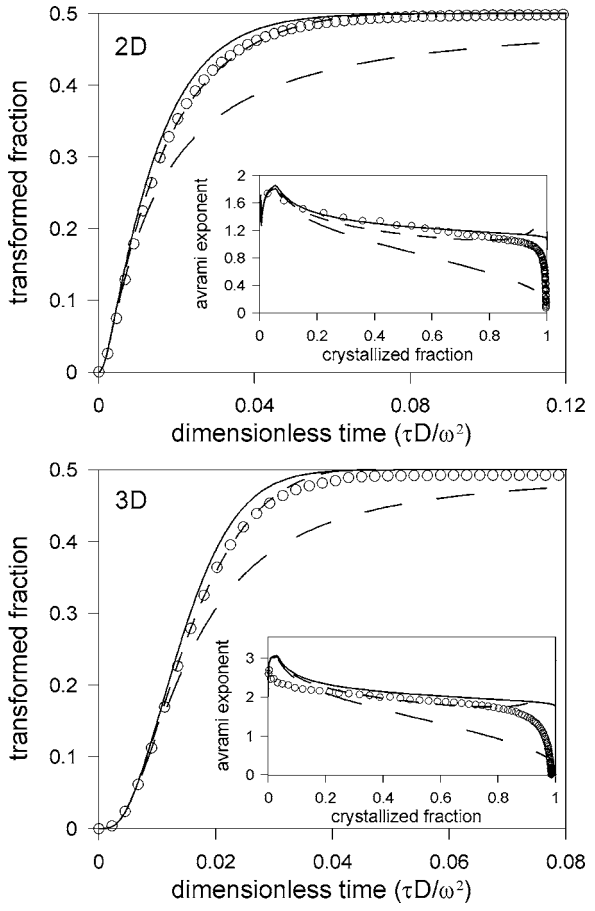

FIG. 8. Transformed fraction and Avrami exponents for transformations with preexisting nuclei and $\gamma=0.5$ in 2D and 3D. Symbols: phase-field simulation; solid line: geometrical model; dashed line: mean-field model; and long-dashed line: geometrical+mean-field model.

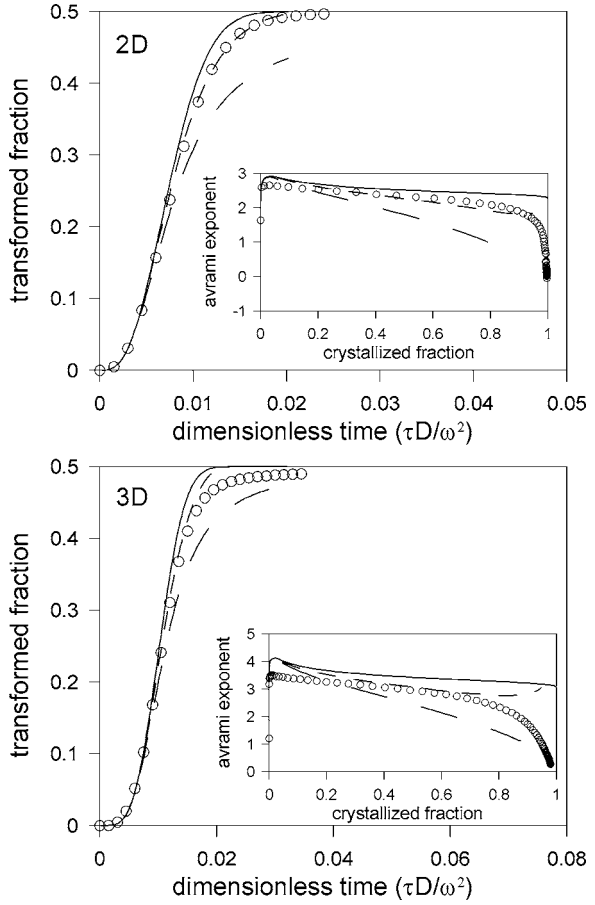

FIG. 9. Transformed fraction and Avrami exponents for transformations with continuos nucleation and $\gamma=0.5$ in 2D and 3D. Symbols: phase-field simulation; solid line: geometrical model; dashed line: mean-field model; and long-dashed line: geometrical+mean-field model.

depending on the value of γ one description is more accurate than the other. The initial values of the Avrami exponent are exactly the theoretically expected: $n=2$ for two dimensions and $n=3$ for three dimensions. These values correspond to a transformation with a constant interface-controlled growth and preexisting nuclei. As the transformation proceeds and the growth becomes diffusion controlled, the Avrami exponent tends to reach the values of 1 and 1.5 for two and three dimensions, respectively. The low n values obtained experimentally in the devitrification of glassy metals are not reproduced by the simulations in any case.

Similar results are obtained in the case of continuous nucleation simulations. Figure 9 shows the results obtained in two- and three-dimensional systems. From the inset figures, it could be observed how the n values evolve from 3 to 2 and from 4 to 2.5 in two and three dimensions, respectively. This corresponds to the change in the growth mechanism from constant interface controlled to diffusion controlled. Again, the Avrami exponent does not reach the low experimental values usually obtained and also given by the geometrical+mean-field model. On the contrary, the two first order approaches describe well the SI effect modeled in the simulations.

Figure 10 shows the particle density evolution $N(t)$ ob-

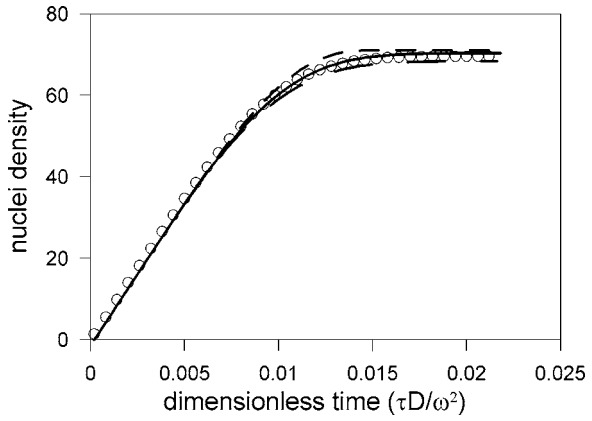

FIG. 10. Particle density evolution. Symbols: phase-field simulation; solid line: geometrical model; and dashed line: mean-field model; and long-dashed line: geometrical+mean-field model.

tained in the three-dimensional simulations and calculated by the kinetic models. The density of particles per unit time throughout the transformation is given by

$$\frac{dN}{dt} = I(c_0)[1 - x_{\mathrm{TB}}(t)] = I_0[1 - \gamma^{-1}x(t)] \tag{36}$$

and

$$\frac{dN}{dt} = I[c_m(t)][1 - x(t)] \tag{37}$$

for the geometrical model and the mean-field model, respectively. In the first case the nucleation frequency is constant but only allowed in the nonstabilized zone of the matrix. In the second case nucleation is allowed in all the untransformed volume but the nucleation frequency is progressively reduced as the mean concentration varies in the matrix. $c_m(t)$ is calculated by means of Eq. (25). Similar to results obtained for $x(t)$ and n both models give a good agreement with the PF simulation. Here it must be remarked that the Q value was chosen to provoke an overall nucleation inhibition equal to that given in the geometrical model. Different values of Q would imply a nucleation inhibition distance different from the thickness δ of the stabilized boundary zone,[26] thus invalidating the use of the simple geometric model described here. On the other hand, the agreement given by the mean-field model is not expected to change in case parameter Q was modified. As stated before, the effect of different nucleation inhibition lengths is considered elsewhere.[35,37]

Simulations with different values of the initial supersaturation γ were performed obtaining the same qualitative results. High γ values imply high concentration gradients and so concentration profiles extend over a small volume fraction making the impingement between grains nearly equivalent to a direct impingement. On the contrary, with low γ values the impingement begins when the distance between neighboring grains is long respect to the grain radius, increasing the importance of the SI effect on the overall kinetics. Figure 11 shows the transformed fraction evolution in two- and three-dimensional preexisting nuclei simulations for $\gamma=0.2$. Comparing with Fig. 8, the bigger effect of the SI is clearly observed. The geometrical and the mean-field models give a

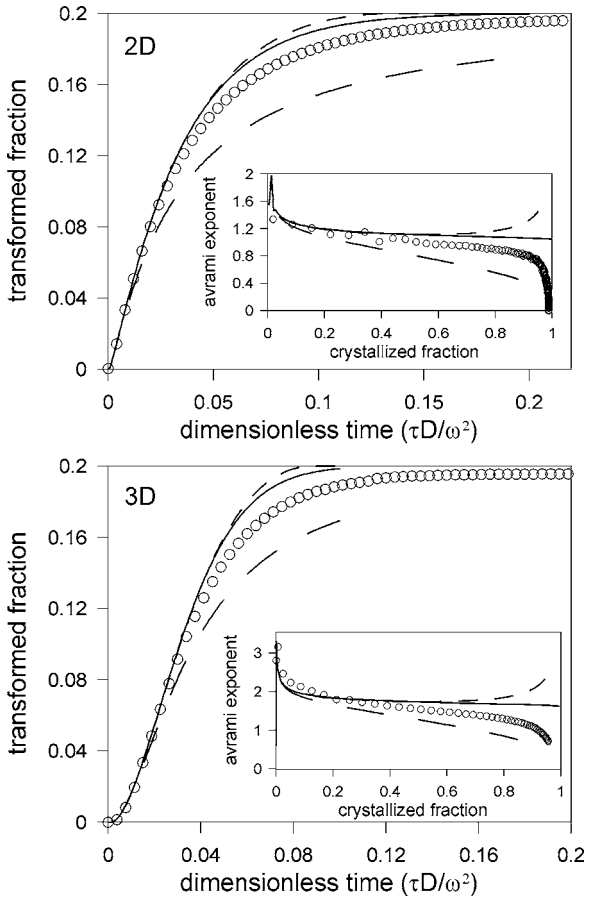

FIG. 11. Transformed fraction and Avrami exponents for transformations with preexisting nuclei and $\gamma=0.2$ in 2D and 3D. Symbols: phase-field simulation; solid line: geometrical model; dashed line: mean-field model; and long-dashed line: geometrical+mean-field model.

good agreement with the simulation up to the half of the transformation; however, at the end both models give faster kinetics with the geometrical model the one closer to the simulations. Similar to the $\gamma=0.5$ case, the geometrical +mean-field model generates kinetics that are slower than the ones obtained from the simulations. The higher degree of deviation between the simulations and the prediction of the kinetic models in the case of $\gamma=0.2$, responds to a lower influence of the geometric impingement than in the case of $\gamma=0.5$. Simulations of transformations with $\gamma>0.5$ cannot be performed with the PF model used in this work because the spheroidal shape of the grains becomes unstable, leading to dendritic growth at the very first stages of the transformation. The spheroidal shape of the grains can be stabilized, reducing the Δx parameter of the simulations; however, this would imply longer computing times. Furthermore, the SI effect in the case of high values of γ is expected to be reduced because of the predominance of the direct impingement. Hence, the approximations based on the KJMA model are expected to reproduce the kinetics of transformations with $\gamma>0.5$ with an agreement at least as good as the one obtained in the $\gamma=0.5$ case.

As already stated, the approximations based on the KJMA model cannot be applied for low γ values ($\gamma \lesssim 0.1$), because the impingement between grains is barely affected by the geometrical distribution of nuclei. In the case of pri-

mary crystallization with higher values of final crystallized volume fraction, this work shows that the first order approximations based on the KJMA model are able to reproduce the kinetics taking into account the SI effect, giving a good agreement in the case of transformations ranging from $\gamma \gtrsim 0.2$ to $\gamma = 1$.

V. CONCLUSIONS

Primary crystallization kinetics was analyzed by means of phase-field model simulations. The model allows to take into account the effects of soft impingement and a concentration-dependent nonrandom nucleation. Usually, these mechanisms were meant to cause the complex kinetics commonly observed in primary crystallization. However, our results show that the classical KJMA model is able to describe the kinetics of the simulations. The Avrami exponent maintains its meaning and the KJMA model normalized by the final crystallized fraction can be used for the evaluation of the growth and nucleation rates, becoming a good first order approach describing the interference between growing particles in the case of soft impingement.

Our results suggest that the delay of the transformation kinetics and the corresponding low Avrami exponent experimentally observed in primary crystallization should not be attributed to the soft-impingement effect. Additional mechanisms have to be considered in order to explain the slowing down of the kinetics as the untransformed matrix becomes progressively stabilized. Further work will be devoted to the study of the effect of the local change in the atomic transport properties of the amorphous matrix due to compositional changes.

ACKNOWLEDGMENTS

This work was funded by CICYT, Grant No. MAT2004-01214, Generalitat de Catalunya, 2005SGR00535, 2005SGR00201, 2005SGR00135, and 2004XT00013, Dirección General de Investigación, BFM2003-07850-C03-02, and Research Training Network, European Commision HPRN-CT-2002-00312.

[1] C. Zener, J. Appl. Phys. **21**, 950 (1949).
[2] H. B. Aaron, D. Fainstein, and G. Kotler, J. Appl. Phys. **41**, 4404 (1970).
[3] W. W. Mullins and R. F. Sekerka, J. Appl. Phys. **34**, 323 (1963).
[4] Y. Couder, J. Maurer, R. González-Cinca, and A. Hernández-Machado, Phys. Rev. E **71**, 031602 (2005).
[5] U. Koster, U. Herold, H. G. Hillenbrand, and J. Denis, J. Mater. Sci. **15**, 2125 (1980).
[6] M. T. Clavaguera-Mora, N. Clavaguera, D. Crespo, and T. Pradell, Prog. Mater. Sci. **47**, 559 (2002).
[7] A. N. Kolmogorov, Dokl. Akad. Nauk SSSR **1**, 355 (1937).
[8] W. A. Johnson and P. A. Mehl, Trans. AIME **135**, 416 (1939).
[9] M. Avrami, J. Chem. Phys. **7**, 1103 (1939); **8**, 212 (1940); **9**, 177 (1941).
[10] J. W. Christian, *The Theory of Transformations in Metals and Alloys* (Pergamon, Oxford, 1975).
[11] T. Pradell, D. Crespo, N. Clavaguera, and M. T. Clavaguera-Mora, J. Phys.: Condens. Matter **10**, 3833 (1998).
[12] A. Korobov, J. Math. Chem. **24**, 261 (1998).
[13] V. Sessa, M. Fanfoni, and M. Tomellini, Phys. Rev. B **54**, 836 (1996).
[14] P. Uebele and H. Hermann, Modell. Simul. Mater. Sci. Eng. **4**, 203 (1996).
[15] E. Pineda, T. Pradell, and D. Crespo, Philos. Mag. A **82**, 107 (2002).
[16] M. P. Shepilov and D. S. Baik, J. Non-Cryst. Solids **171**, 141 (1994).
[17] D. P. Birnie and M. C. Weinberg, J. Chem. Phys. **103**, 3742 (1995).
[18] F. S. Ham, J. Phys. Chem. Solids **6**, 335 (1958).
[19] J. W. Cahn, Acta Metall. **4**, 449 (1956).
[20] K. F. Kelton, J. Non-Cryst. Solids **163**, 283 (1993).
[21] O. R. Myhr and O. Grong, Acta Mater. **48**, 1605 (2000).
[22] D. R. Uhlmann, J. Non-Cryst. Solids **7**, 337 (1972).
[23] D. Hampel, A. Pundt, and J. Hesse, J. Phys.: Condens. Matter **4**, 3195 (1992).
[24] A. Cserei, J. Jiang, F. Aubertin, and U. Gonser, J. Mater. Sci. **29**, 1213 (1994).
[25] D. Jacovkis, Y. Xiao, J. Rodriguez-Viejo, M. T. Clavaguera-Mora, and N. Clavaguera, Acta Mater. **52**, 2819 (2004).
[26] M. P. Shepilov, J. Non-Cryst. Solids **208**, 64 (1996).
[27] D. R. Allen, J. C. Foley, and J. H. Perepezko, Acta Mater. **46**, 431 (1997).
[28] H. Hermann, Europhys. Lett. **41**, 245 (1998).
[29] H. Hermann, Europhys. Lett. **51**, 127 (2000).
[30] R. González-Cinca, L. Ramírez-Piscina, J. Casademunt, and A. Hernández-Machado, Phys. Rev. E **63**, 051602 (2001).
[31] S. L. Wang, R. F. Sekerka, A. A. Wheeler, B. T. Murray, S. R. Coriell, R. J. Braun, and G. B. McFadden, Physica D **69**, 189 (1993).
[32] L. Granasy, T. Pusztai, and J. A. Warren, J. Phys.: Condens. Matter **16**, R1205 (2004).
[33] K. R. Elder and M. Grant, Phys. Rev. E **70**, 051605 (2004).
[34] S. Chan, J. Chem. Phys. **67**, 5755 (1977).
[35] P. Bruna, Ph.D. thesis, Universitat Politècnica de Catalunya.
[36] J. D. Gunton, J. Stat. Phys. **95**, 903 (1999).
[37] E. Pineda and D. Crespo, J. Non-Cryst. Solids **317**, 85 (2003).
[38] E. Pineda, P. Bruna, and D. Crespo, Philos. Mag. **84**, 2023 (2004).
[39] E. Pineda, P. Bruna, and D. Crespo, Phys. Rev. E **70**, 066119 (2004).